ELSEVIER

Catalysis Today 44 (1998) 3–16

CATALYSIS TODAY

Chemical preparation and characterization of metal–metalloid ultrafine amorphous alloy particles

Yi Chen*

Institute of Mesoscopic Solid State Chemistry, Department of Chemistry, Nanjing University, Nanjing 210093, China

Abstract

Ultrafine amorphous alloy particles (UAAP) constitute an overlapping area of amorphous alloys and nanophase materials. Special properties of the particles derived from the combination of their long-range disordered structure and nanoscale size are of great interest in catalysis. This paper reviews some fundamental aspects in the chemical preparation of UAAP consisting of transition metal (M) and metalloid elements (B, P) and their applications in catalysis. The three fundamental reaction equations in the preparation of MB UAAP, the autocatalytic nature of the chemical reaction to produce NiP UAAP, and a milling-induced solid state reduction method are discussed. Their interesting catalytic properties, especially their unique selectivities in some of the hydrogenation reactions, have shown promising potential applications of UAAP in catalysis. With regard to the interactions between the transition metal and metalloid elements of the UAAP, experimental results and theoretical calculations have led to the suggestion that the charge transfers between M and B or P are in the same direction but to different extents, i.e., from metal to metalloid elements.

Keywords: Ultrafine particles; Amorphous alloy; Metal-metalloid catalyst

1. Introduction

Amorphous alloys [1,2] and nanophase materials [3,4] have attracted much attention in the past two decades. They are expected to have special properties and in fact they have found important practical or potential applications in various fields, such as in powder metallurgy, magnetic recording media, ferrofluids, composite materials, and catalysis. By the combination of the unique attributes of the amorphous alloys, i.e., the short-range order and long-range disorder in structure, and the ultrafine size of the nanophase materials, UAAP (ultrafine amorphous alloy particles) constitute an overlapping region of the above two active fields – an interdisciplinary area full of challenge. Chemical reduction method has its own advantages in the preparation of UAAP. In contrast to the melt-quenching method [5], the composition and hence the properties of the UAAP are more adjustable, i.e., the ratio of different elements in the product is not limited nearly to the eutectic composition of the alloy. Moreover, in comparison with ribbon samples, UAAP prepared by chemical reduction have higher specific surface area and are easier to be suspended in liquid phase or compacted to appropriate shapes [6]. It has been reported that in catalysis only mild pretreatments are required for the activation of UAAP [7]; moreover, chemical reduction methods might have significant potential for large-scale production [8].

*Corresponding author. Tel: 00 86 25 360 4633; fax: 00 86 25 330 2728; e-mail: chenyi@nju.edu.cn

0920-5861/98/$32.00
PII S0920-5861(98)00169-2

Although the reduction of transition metal ions by borohydride dates back to investigations during the 1950s [9], increasing attention has been drawn to these reactions by recognizing their significance and complexity [10,11]. A variety of UAAP consisting of transition metal (M) and metalloid elements (B, P) as well as nanoscale metal or metal–metalloid crystalline particles have been prepared by chemical reduction and characterized by various techniques. Examples of UAAP include MB (M=Fe, Co or Ni) [6,11–13], NiP [7,14–19], CoP [19], FePB [20–22], NiPB [23], FeMB (M=Cr, Mn, Co or Ni) [5], FeNiB [5,21,24,25], NiCoB [26–28], NiWP [29] as well as ultrafine crystalline particles of Co, Co_2B or $Co(BO_2)_2$, and Fe, Fe_2B, Mg, Al, Ni, Pd, and Cu [30]. By controlling reaction conditions amorphous or crystalline nanoscale particles, typically in the range around 10–100 nm, can be obtained. It has been well recognized that the reaction conditions have significant effects on the properties of the UAAP. However, the detailed chemistry of these reactions is not yet well understood, and there are examples that small changes in the preparation procedures can cause the product to be completely different [30].

In the past decade extensive work has been devoted to understanding the reaction mechanism and the key factors in the preparation of UAAP which influence the composition, structure, morphology, and hence the properties of the particles. The advancements in these respects might finally lead to the controlling and tailoring of the properties of the UAAP prepared and also to the finding of new materials which either have novel properties or are more economic and efficient than their conventional counterparts. Understanding of the relationships between the structure, morphology, composition and properties of the UAAP, is important both in practical applications and fundamental studies, as it has been argued that due to the unique features of these kinds of materials neither quantum chemistry nor non-classical law of solid state physics can directly be applied [30]. This paper attempts to discuss some recent results on the chemical preparation and characterization of the UAAP consisting of transition metal and metalloid elements. Emphasis will be placed on binary systems since it is reasonable to address the complicated tasks for relatively simple systems, which in fact provide a framework for the understanding of other more complicated systems.

2. Chemical preparation of ultrafine amorphous alloy particles

The most widely investigated method for the production of MB UAAP is the reaction of transition metal ions such as iron, cobalt or nickel in aqueous solution with KBH_4. It has been observed from practical experience that metal ions with their E^0 (standard electrode potential) values lower than about -1.0 V are not reducible by BH_4^- in aqueous solution, Fe^{2+}, Fe^{3+}, Co^{2+}, Ni^{2+}, Cu^{+}, Cu^{2+}, Ag^{+}, Au^{+}, Au^{3+}, Pt^{2+}, Pd^{2+} Ru^{3+}, Rh^{3+}, Os^{3+} and Ir^{3+} cations are on the list of ions which can be reduced to metal or metal borides by BH_4^- [30], and one can see that quite a few of the above metals are important for catalysis. A series of studies have been performed to elucidate the influences of reaction conditions, such as concentration and ratio of the reactants, pH value of the solution, mixing procedures and reaction temperatures, etc., on the properties of the UAAP. A diversity of results can be found in the literature. For example, it has been claimed that the most important preparation parameters which influence the composition of the UAAP of Fe–B are the concentration of borohydride solution and the pH of the transition metal salt solution [6], and it has also been reported that for a similar system the mole ratio of KBH_4 to the metal ions plays a critical role in determining the structure (amorphous or crystallites), morphology (spherical or chain-like particles) and composition (B content in UAAP decreases with the increase of the ratio) [11].

2.1. *Fundamental reactions for the preparation of MB by chemical reduction*

Various reaction equations have been proposed to describe the interaction of borohydride and transition metal ions in aqueous solution [31,32]. Kinetic studies on the reactions carried out by adding potassium borohydride solution at a constant speed into aqueous solutions of $FeSO_4$, $CoCl_2$ or $NiCl_2$, respectively, have proved that all the proposed reaction equations concerning this reaction can be obtained by linear combination of the following three independent

equations [12]:

$$BH_4^- + 2H_2O \rightarrow BO_2^- + 4H_2 \quad (1)$$

$$BH_4^- + 2M^{2+} + 2H_2O \rightarrow 2M + BO_2^- + 4H^+ + 2H_2 \quad (2)$$

$$BH_4^- + H_2O \rightarrow B + OH^- + 2.5H_2 \quad (3)$$

Thus, if one can estimate the influence of the reaction conditions on the relative contribution of the above three independent equations to the overall reaction, then it might become possible to predict the effect of reaction conditions on the composition of the UAAP prepared.

Shown in Fig. 1 is a representative curve of the variation of the pH value of the solution with reaction time. A plateau on the curve indicates that the pH value of the solution automatically maintains a constant level during the reduction reaction.

The results are consistent with the above three equations. By adding BH_4^- into the acidic $FeSO_4$ solution, Eq. (1) will proceed first because the electrode potential of H^+/H_2 is apparently higher than that of Fe^{2+}/Fe. As can be seen from Fig. 1, the consumption of H^+ during the hydrolysis of KBH_4 results in a dramatic increase of the pH value of the solution until the electrode potentials of H^+/H_2 and Fe^{2+}/Fe cross and the reduction of Fe^{2+} ions begins. Due to the hydrolysis of BO_2^-, Eq. (1) is in fact equivalent to the following equation:

$$BH_4^- + 3H_2O \rightarrow HBO_2 + 3H_2 + OH^- \quad (4)$$

in which the influence of the hydrolysis of BH_4^- on the pH value of the solution can clearly be seen. The reduction of Fe^{2+}, as shown by Eq. (2), produces H^+ and metal Fe, and the UAAP of FeB are formed by the interaction of the metal Fe and boron atoms produced by reaction (3) which is induced by the metal atoms in solution. Noticeably, the production of H^+ according to Eq. (2) will lead to the decrease of the pH value of the solution, but the participation of reaction (3) has an opposite effect similar to that of Eq. (1), i.e., to increase the pH value of the solution. The combination of reactions (1)–(3) explains the existence of the plateau at pH value around 4.30, which remains almost a constant throughout the reaction for the production of FeB UAAP. As soon as all the metal ions in solution are reduced, the addition of KBH_4 will cause another abrupt increase of pH value due to the hydrolysis of the extra amount of KBH_4 added.

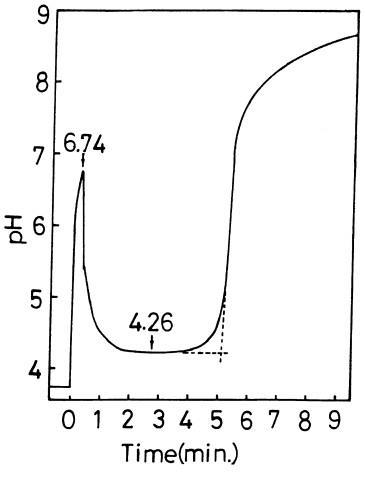

Fig. 1. The variation of pH value versus time by adding potassium borohydride solution (0.5 M, pH=12) to ferrous sulfate solution (200 ml, 0.1 M) at a constant speed (from [12]).

Equations have been derived to evaluate the effect of some of the reaction parameters, i.e., the concentration of KBH_4 solutions and their adding speed, on the relative contribution of the three independent reactions. From the relative contribution of reaction (2) to reaction (3), the composition of product, i.e., the M/B ratio, can be estimated, and from the relative contribution of Eq. (1) the effect of the hydrolysis of borohydride to produce oxides of boron can be evaluated. Eq. (1) leads to the formation of the undesirable by-product, i.e., boron oxides, and the waste of reducing reagent, which seems to be an inevitable side reaction in aqueous solution. The results calculated based on the measurements of the volumes of hydrogen evolved and the amount KBH_4 consumed upon reaching the equivalent point of the reaction (as shown in Fig. 1) are listed in Table 1. The calculation and experimental results are consistent, and it has been found that similar agreement holds true for the preparation of CoB and NiB UAAP under different KBH_4 concentrations and adding rates. The consistency in experimental and predicted results indicates that the above mechanistic consideration has captured the essentials of the reduction reactions. Two important conclusions can be drawn from Table 1. First, the molar ratio of KBH_4/M^{2+} is around 1.8–1.9 at the equivalent point of the reaction, and thus it is not

Table 1
Experimental results for preparing FeB UAAP with different adding rates (Time/142 ml) of KBH_4 solutions [12][a]

Time (min)	*A*	*B*	$B^*_{predicted}$	B^*_{ICP}	*l*:*m*:*n*	*l*:(*l*+*m*+*n*) (%)
5.00	3.126	2.609	35.0	18.7	1.91:0.93:1	49.8
9.43	3.252	1.910	22.2	22.7	3.93:1.75:1	58.9
23.45	3.194	1.838	24.3	24.8	3.17:1.56:1	55.3
31.43	3.213	1.921	25.4	25.8	3.16:1.47:1	56.2
40.50	3.128	1.869	29.6	28.6	2.26:1.19:1	50.8
55.10	3.152	1.925	29.7	28.5	2.38:1.19:1	52.1

[a]Symbol *A* denotes moles of H_2 released by the consumption of 1 mol KBH_4; while *B* denotes moles of KBH_4 consumed for the reduction of 1 mol Fe^{2+}. B^*s: Predicted boron content in the sample measured by ICP, respectively. *l*, *m* and *n* are factors of reaction (1), (2) and (3) in the overall reaction, respectively. The relations between *A*, *B* and *l*, *m*, *n* have been derived in [12].

necessary to use a molar ratio much higher than 2 as adopted in some literature. Second, about 50% of KBH_4 are hydrolyzed to produce boron oxides during the reaction, which is the shortcoming but seems inevitable for the reaction carried out in aqueous solution.

Further studies have shown that similar mechanistic considerations can also be applied to the case of reverse addition of solutions, i.e., adding Fe^{2+} solution (3.71×10^{-4}–0.94×10^{-4} mol/l) into the aqueous solution of KBH_4 (0.06 mol in 200 ml, pH=12) so as to produce FeB. However, as the reaction is carried out in a basic medium, the pH value of the solution dropped rapidly at first, and then due to the balance of the related equations discussed above, the pH value soon reached a constant value which is maintained to the end of the reaction, and which was found to be a value in the range 8.5–9.5 depending on the concentrations of the $FeSO_4$ solution used [33].

It has been pointed out in the literature that the concentration of borohydride is an important parameter to influence the composition and morphology of the particles. It was reviewed by Linderoth and Mørup in the early 1990s [6,12], for the dropwise addition of BH_4^- to iron salt solution that has the molarity of borohydride solution decreases, the amount of the crystalline component in Fe–B alloy decreases, and finally UAAP of Fe–B containing 28–33 at% of B can be formed. By mixing the solutions of BH_4^- and iron salts with a Y junction, increasing the concentration of borohydride will cause an increase of boron content and a decrease of the particle size of CoB. On the other hand, for dropwise addition of iron salt solution into borohydride aqueous solution, the concentration of the borohydride does not have any systematic influence in producing UAAP of Fe–B with 32–37 at%. By adding KBH_4 aqueous solution into metal (Fe, Co or Ni) salt solution, Saida et al. [11] have also found that the B content in the UAAP of FeB increases with the increase of the ratio of KBH_4 to metal ions, but the molar ratio has little effect on the B contents in the UAAP of CoB or NiB samples. Moreover, the structure of the UAAP was found to change from amorphous to crystalline when the molar ratio decreased. The influence of reduction temperatures on the size of the UAAP has been the subject of several investigations. The decrease of the particle size of the UAAP with the increase of the reduction temperature, and the oxidation of the products at high reduction temperature as well as the inclusion of unreacted reduction reagent at low temperature have been observed [6,11,24]. Recently, it has been found that the reduction temperature has a pronounced effect on the composition of UAAP, e.g., by changing the reduction temperature from -7°C to 30°C, the B content in FeB UAAP can be adjusted in a range as wide as 23–40 at% [34]. As the nature of the products is influenced by multiple factors, e.g., different ways and rates of mixing the related solutions, concentration and the ratio of the reactants, pH value of the reaction solution, and the reduction temperature, etc., it seems impossible to discuss the role of a single parameter in detail.

2.2. *Preparation of FeB UAAP by milling-induced solid state reduction*

The reduction of metal salts by alkali or alkaline metals, e.g., Na, K, or Ca, has been reported either in non-aqueous solution using a polar organic solvent

[35] or through the mechanical milling of their mixtures [8] to produce nanosize CoB, FeB and CuB particles. The high reducing potential of the alkali or alkaline metal makes it possible to obtain metals, e.g., Mg, Al, In, etc., from their salts which cannot be reduced by borohydride in aqueous solutions. Moreover, since water is not present during milling, the hydrolysis of the reducing reagent can be avoided, and hence the amounts of oxide by-products as well as the reducing reagent consumed by the side reaction can be reduced. However, the organic solvents and the alkali or alkaline metal used in the above reactions are not only expensive but also complicated to handle. Recently, a milling-induced solid state reduction method to produce ultrafine amorphous particles has been developed [36]. Taking the reduction of anhydrous $FeCl_3$ by KBH_4, for example, a mixture with $FeCl_3$ to KBH_4 ratio of 1:3.3 was loaded into the grinding vial in a glove box filled with high purity Ar and was milled for about 3.5 h, followed by annealing under Ar atmosphere at a temperature lower than the glass transition temperature of the product. Mössbauer spectroscopy was used to monitor the milling-induced chemical changes. Shown in Fig. 2 are the Mössbauer spectra of samples after different periods of milling, and the relative spectral areas of the coexistence species in the mixture are computer-fitted and presented in Fig. 3. The milling-induced reaction consists of two steps, namely, the reduction of Fe^{3+} to high spin Fe^{2+} species (Fe^{2+}–A) in about 30 min, and then it was gradually converted to another Fe^{2+} species (Fe^{2+}–C) during milling, which is tentatively assigned to low spin Fe^{2+} species according to its Mössbauer parameters:

$$FeCl_3(IS = 0.437\,mm/s) \rightarrow Fe^{2+}\text{–A}(IS \approx 0.31\,mm/s,\ QS \approx 1.50\,mm/s,\ 0.5\,h)$$

$$\rightarrow (Fe^{2+}\text{–C}(IS \approx 0.238\,mm/s,\ QS \approx 0.60\,mm/s,\ 3\,h)$$

After milling, the mixture was annealed at 673 K to further reduce the Fe^{2+} species with the formation of ultrafine amorphous $Fe_{49}B_{51}$ spherical particles, which have a surface area of about 61 m^2/g and a size around 10 nm. Increasing the annealing temperature, say, to 1073 K, will lead to the formation of crystalline α-FeB particles. A two-step reduction process, i.e., the presence of $FeCl_2$ after short milling

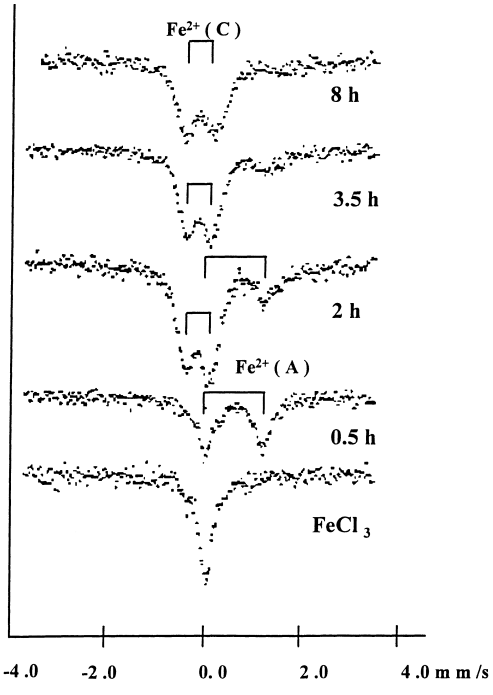

Fig. 2. Mössbauer spectra of $FeCl_3$ and the mixture of KBH_4 and $FeCl_3$ after milling for various periods of time.

times, have also been reported in the literature, where $FeCl_3$ and Na interacted to give the final products of α-Fe particles and a small amount of unreduced $FeCl_3$ [8]. To the best of our knowledge, such a high boron content and high surface area FeB sample cannot be produced by reduction in aqueous solutions. Preliminary results have shown that by adjusting reaction conditions, FeB (45–55 at%), CoB (20–28%) and

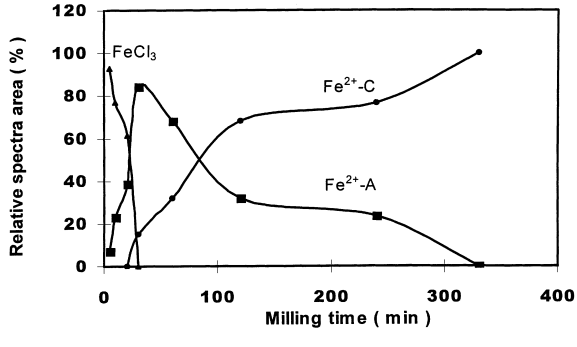

Fig. 3. Relative amounts of $FeCl_3$ and various Fe^{2+} species versus milling time.

NiB (9–25%) amorphous nanoscale particles can be prepared. The results demonstrate that the milling-induced and the annealing processes can be completed in a reasonably short time and at moderate temperatures. Therefore, this preparation method has indeed the potential for the large-scale production of a wide range of ultrafine amorphous or crystalline materials with comparably high yield rates and low costs [37].

2.3. The autocatalytic nature of the NiP preparation

As it is, studies of NiP amorphous alloy catalysts for hydrogenation dates back to the early 1970s, and supported NiP catalysts have been prepared and characterized [19,38,39]. In fact, to incite the reduction of Ni^{2+} ions by sodium hypophosphite in aqueous solution to produce NiP amorphous film has long been used in electrolytic plating. By conventional methods, the reaction can only be performed at $\geq$351 K, and a period of time was needed to initiate the reduction, which could be finished rapidly after the appearance of the black precipitates [40,41]. The autocatalytic nature of the above reaction has been reported recently [16,18]. In short, a drop of KBH_4 solution is added to a mixture containing appropriate amounts of $NiCl_2{\cdot}6H_2O$, $NaH_2PO_4{\cdot}H_2O$ and $Na_3C_6H_5O_7{\cdot}H_2O$, which has a pH value of 9.2 adjusted by adding a sodium hydroxide solution, after an incubation period the autocatalytic reaction takes place at room temperature. Shown in Fig. 4 are the curves of the volumes of evolved hydrogen and the pH values of the solution measured at different reaction times. The sigmoid curve of the evolved hydrogen versus time reveals the autocatalytic nature of the reaction. An incubation period for creating catalyst particles is reflected on the flat line of the curve before the catalytic reaction to produce hydrogen begins, and this explains the fact that heating was often needed to induce the reaction if there were no KBH_4 added. Moreover, based on mechanistic studies, the overall reaction of the production of NiP is suggested to be composed of the following three independent reactions:

$$Ni^{2+} + H_2PO_2^- + H_2O \rightarrow H_2PO_3^- + 2H^+ + Ni \quad (5)$$

$$3H_2PO_2^- \rightarrow H_2PO_3^- + 2P + H_2O + 2OH^- \quad (6)$$

$$H_2PO_2^- + H_2O \rightarrow H_2PO_3^- + H_2 \quad (7)$$

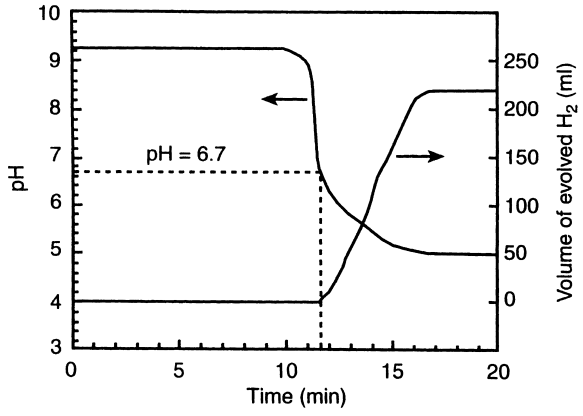

Fig. 4. The pH value of the solution and volume of evolved H_2 versus time for reaction between nickel chloride and sodium hypophosphite in aqueous solution at room temperature.

As shown in Fig. 4, the initial pH value of the solution was about 9.2, in which the Ni^{2+} ions should have had the form of $Ni(OH)_2$. By adding a drop of KBH_4 solution and after about 10 min incubation period, the pH value of the solution dropped rapidly because of the reduction of Ni^{2+} which produced H^+ as shown by Eq. (5). When the pH value dropped to about 6.7, the dissolving of $Ni(OH)_2$ as well as the reaction of Eq. (6) might slow down the decrease of pH value of the solution, and meanwhile large amounts of H_2 evolved due to the hydrolysis of $H_2PO_2^-$ as depicted by Eq. (7) catalyzed by the NiP UAAP formed. Finally, the reactions ended in several minutes after the pH value of the solution dropped to about 5, and the hypophosphite ions were reacted.

The rate of H_2 evolved can be expressed as

$$dV_{H_2}/dt = K'[H_2PO_2^-]S, \quad (8)$$

where S is the surface area of the NiP product. The integration of Eq. (8) is in good consistency with the experimental data. Electron diffraction and TEM have proved the formation of spherical amorphous $Ni_{85}P_{15}$ particles with a uniform size of around 100 nm. It has been found that the incubation period increases with the increase of pH value of the solution, e.g., which goes up to about 30 min when the pH value increases to 11 (41). Generally the reaction can be completed in the pH range 8–12 and about 56% of the hypophosphite are consumed in the hydrolysis of sodium hypophosphite as shown by Eq. (7). Thus, similar

to the preparation of FeB UAAP, the hydrolysis of the reducing agent also seems to be inevitable for the preparation of NiP UAAP in aqueous solution. The P content in NiP can increase by lowering the reaction temperature or increasing the concentration of the reactants. In fact, NiP UAAP with P content 9–24 at% have been prepared and crystalline nickel was found in the samples containing P≤9 at% [18].

2.4. Ternary UAAP prepared by chemical reduction

Ternary UAAP, i.e., M_1M_2B (or P) or MBP, have been the topics of current investigations, as it is expected that the properties of the UAAP can be further tailored by the combination of different elements. These tri-component UAAP were prepared by the reaction of KBH_4 aqueous solution with solution containing the related metal salts or metal salt plus sodium hypophosphite. It has been found that by adding $NaBH_4$ solution to a solution containing $FeSO_4$ and $NiCl_2$, the amorphous UAAP of FeNiB can be obtained at 100% yield only when the pH value and the concentration of sodium borohydride were controlled in a certain range, i.e., pH=5–6.5 and concentration around 0.10–0.15 M, respectively [25]. The atomic ratios of M_1 to M_2 or B to P in the particles prepared can be adjusted by controlling reaction conditions, e.g., the concentration of the alkaline borohydride, the ratio of metal salts and the pH value of the reaction solution [22,27]. It is interesting to note that, for UAAP of FeNiB [24,42] and FeCoB [5], the ratios of metal components in the UAAP are close to those of the corresponding solutions. Shown in Fig. 5 is the relationship between the Ni (Ni+Fe) ratios of the 0.1 M ($FeSO_4$+$NiCl_2$) solutions and the FeNiB UAAP samples obtained by dropwise addition of 100 ml 1 M KOH to 100 ml of the above solutions under vigorous stirring for 10 min at 0°C. Since the composition of the solution, i.e., the relative amount of Ni^{2+} and Fe^{2+} ions, is easily adjustable, the relative amount of the metal components in the UAAP can thus be altered over a wide range. This unique characteristic makes the adjustment of some properties of the UAAP possible. For example, by adjusting the ratio of Ni to (Ni+Fe), the magnetic properties of FeNiB can be modified dramatically [24].

The successful preparation of UAAP that contain both P and B as metalloid constituents also provides the possibility of composition variation to improve their physical and chemical properties. The preparation and characterization of FePB [20] and NiPB [23] UAAP have been reported in detail [20,23]. It has been demonstrated that the tri-component NiPB alloy particles have higher amorphous structural stability than NiP or NiB alloys [43].

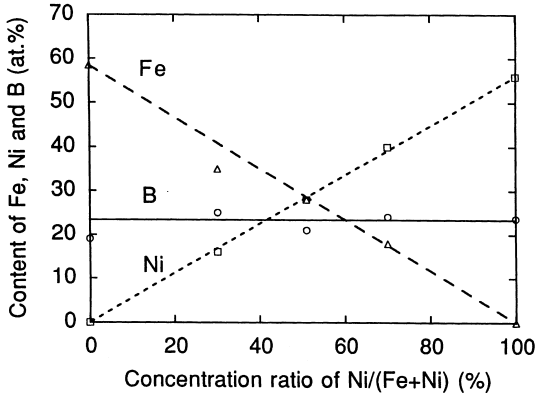

Fig. 5. The relationship between the Ni^{2+}: (Ni^{2+}+Fe^{2+}) ratios of the 0.1 M ($FeSO_4$+$NiCl_2$) solutions and the FeNiB UAAP samples obtained.

3. Interaction of metal–metalloid elements in the ultrafine amorphous alloy particles

To understand the nature of the interactions between the transition metal and metalloid elements is of great importance to the possible control of the properties of UAAP. Many studies have addressed on the influences of P or B on the electronic state of the metal elements, which obviously should have significant effects on some of the properties, e.g., magnetic and catalytic properties, of the UAAP. Even though various techniques have been applied in these studies, the exact nature of the interaction is not yet clear, and controversies on the explanation of the experimental results can be found in the literature.

It has been suggested that electrons are transferred from P or B to the d band of transition metals in amorphous alloys, and comparatively P has a stronger tendency to donate electrons as revealed by magnetic studies [44,45]. In contrast, it has been proposed that nickel accepts electrons from boron but gives electron to phosphorus based on the changes of the binding

energies of B and P, whereas no appreciable change on the binding energy of Ni_{2p} has been detected [39,46,47]. By analyzing the peak shapes of XPS profiles of NiB and NiP amorphous alloys with different nickel contents, it has been argued that for NiB, nickel accepts electrons from boron but for NiP, depending on its composition, nickel might either accept electrons from P for samples containing Ni≥75% or donate electron to P for samples with low Ni content [48–50].

Different suggestions on the direction of charge transfer between metal and metalloid elements have been proposed. However, all experimental results point to the fact that the binding energy of M (M=Ni, Fe, Co,. . .) in the UAAP is the same as that of the pure metal, and various oxide species, i.e., oxides of B, P and M, have been detected on the surface. It is quite common in the literature to suggest that electrons are transferred from boron to Ni and from Ni to phosphorous in samples of NiB and NiP, respectively. However, from the chemical point of view, it is hard to accept that B and P could have such big differences in their electron affinity, i.e., one donates electrons to and one accepts electrons from nickel, as B and P both have a higher electronegativity than that of Ni. To provide a deeper insight into the interaction, the activation energy of ethylene hydrogenation and the differential heat of CO chemisorption are used as chemical probes to compare the surface electronic state of the $Ni_{68}B_{32}$ and $Ni_{83}P_{17}$ samples. Apparently, if the electronic effects of B and P on nickel were in opposite directions, then the activation energies and the heat of adsorption of the NiB and NiP samples would, accordingly, have gone in opposite directions. Thus, if one is larger than that of nickel, the other should be smaller and vice versa.

The results shown in Table 2 demonstrate that the activation energies of the hydrogenation of ethylene and the initial differential heat of adsorption of CO on NiB and NiP are lower in comparison with those of pure metal Ni. The activation energy (E_a) and pre-exponential factor (A_s) of each catalyst were obtained from the slope and intercept of the $\ln K_s \sim 1/T$ plot where K_s is the rate constant of ethylene hydrogenation reaction and T is the reaction temperature [51]. A mixture of $C_2H_2+H_2$ (with a volume ratio of 1:1) was pulse-injected into the reaction tube containing 0.1–0.6 g catalyst at a temperature in the range 20–150°C. Helium was used as the carrier gas at a flow rate of 0.43 ml/s, and the injection rate of the gas mixture was 2.36 ml/10 min. An on-line GC with a Poropak QS column operated at 150°C was used to analyze the products. The data of heat of adsorption were measured at 308 K and all the samples were reduced at 623 K before measurement [52], the crystallization of the amorphous samples was assumed to have no significant effect on the nature of the electronic interactions between the elements.

The XPS results of the above samples are shown in Table 3. The peaks with lower binding energies in B_{1s} and P_{2p} are usually assigned to atomic metalloid elements bound to Ni, i.e., species Bn (B_{1s}=188.2 eV) and Pn (P_{2p}=129.3 eV), respectively. And those higher binding energy peaks are assigned to the oxidized species Bo (B_{1s}=191.8 eV) and Po (P_{2p}=132.6 eV), respectively. It has been well established in the literature that the oxidized species come from the hydrolysis of BH_4^- and $H_2PO_2^{2-}$ are hard to remove, even though the sample was thoroughly washed [46]. As shown in Table 3, the binding energy of atomic P in UAAP is lower than that of pure red phosphorus suggesting that P accepted negative charges from Ni atoms to make it more electron-deficient. It is known that H_2 is easy to dissociate on the electron-deficient Ni centers [53]. The fact that the hydrogenation activation energy of NiP is lower

Table 2
The apparent activation energy (E_a) and the pre-exponential factor (A_s) of ethylene hydrogenation [51], and the initial differential heat of CO adsorption (Q_a) [52] on Ni, NiB and NiP samples

Catalyst	E_a (kJ/mol)	A_s	Q_a (kJ/mol)
Ni (powder)	34	9.5×10^5	12
$Ni_{68}B_{32}$ (UAAP)	12	1.5×10^4	10
$Ni_{83}P_{17}$ (UAAP)	7.7	8.6	92

Table 3
Binding energy (eV) of various species on NiB and NiP UAAP [51]

Sample	$Ni2p_{3/2}$	B_{1s} (Bn)	B_{1s} (Bo)	P_{2p} (Pn)	P_{2p} (Po)
$Ni_{68}B_{32}$	852.9	188.2	191.8		
$Ni_{83}P_{17}$	853.0			129.3	132.6
Ni	852.8				
Pure B		187.5			
Pure P				130.4	

than that of pure Ni, as shown in Table 2, seems to support the above consideration, i.e., negative charges were transferred from Ni to P in the UAAP of NiP.

While the conclusions on the interaction between P and Ni are consistent in most of the literature, the interaction between B and Ni seems different. It seems reasonable to argue that the increase of its binding energy only indicates that negative charges have been withdrawn from B atoms. No decisive evidence or reason can be used to support the idea that the charges from B should go to Ni atoms, as no change in the binding energy of Ni has been observed. It has been suggested that Ni–P–O species with a P/Ni=0.38 are present on the surface of supported NiP sample [19], and XPS results have confirmed that the existence of oxide species is inevitable on NiB UAAP prepared by chemical reduction. It is suggested that electron transfer from B to its nearest oxygen containing species seems more plausible. As reflected in Table 2, the experimental results on the hydrogenation activation energy and the heat of adsorption of CO have shown that the role of B is similar to that of P, i.e., their effects on the electronic state of Ni are in the same direction to different extents.

It is hoped that the dilemma concerning the transfer of electrons between the metalloid elements and the metal can be better understood by analyzing the local surface electronic state of the Ni, NiB and NiP samples [51]. The self-consistent charged–discrete variation Xα(SCC–DV–Xα) method has been applied and some of the results are listed in Table 4. The calculation results provide insight into the influence of metalloid elements on the electron population in different orbitals as well as on the net charge of the metal. In comparison with pure Ni, one can see from the table that the electron densities of nickel 3d orbital in NiB and NiP increase, while those of s plus p orbitals decrease. The addition of metalloid elements results in the lowering of the energy, E (total), and the increase of the net charge at Ni, i.e., the net effect of the interaction is the transfer of electrons from Ni to the metalloid element. However, the excitation of nickel's 4sp electrons to 3d orbital might cause the increase of its electron density.

Similar calculations on M(Fe or Ni)PB samples have demonstrated that the interaction between P and M is stronger than that of B, and the interaction between B and P in the alloy can be neglected [54].

Table 4
SCC–DV–Xα calculation results of the surface Ni in Ni, NiB and NiP samples [51]

	Ni	NiB	NiP
Orbital population			
3d	8.4399	8.4481	8.4438
4s	1.0407	1.0214	0.8410
4p	0.4533	0.4284	0.5199
Net charge at Ni (n)	0.06602	0.10219	0.19529
$-E_{total}$ (a.u.)	377.5147	388.4854	395.4159

4. The catalytic properties of metal–metalloid ultrafine amorphous alloy particles

Examples of amorphous alloys prepared by rapid quenching methods with better catalytic properties than their crystalline counterparts were reviewed by the end of the 1980s [2]. Almost at the same period, the superior catalytic properties of UAAP have also been recognized. For example, NiB UAAP exhibits high resistivity to poisoning as well as good activity and selectivity for certain hydrogenation reactions, and NiP UAAP displays specific selectivity for some reactions in spite of the relatively low activity [39]. In fact, it is known that amorphous NiP ribbon is more active than the corresponding crystallized NiP or Ni foil for the hydrogenation of styrene [55], and NiP UAAP are even better than NiP ribbon. Fig. 6 shows the facts that a $Ni_{85}P_{15}$ UAAP sample gives 100% conversion and selectivity for the hydrogenation of styrene to ethyl benzene at 160°C and a liquid space velocity of 46 h^{-1}, and the catalyst is stable for more than 40 h. In contrast, a ribbon sample with similar composition, i.e., $Ni_{87}P_{13}$, requires higher reaction temperature (280°C) and lower liquid space velocity (6 h^{-1}) to reach the similar conversion, and even worse, its activity decreases dramatically after 3 h on stream [7]. Moreover, complicated pretreatment conditions, e.g., treated with acid, and followed by oxidation and reduction at high temperature by oxygen and hydrogen, respectively, are often needed for the activation of the ribbon samples [2,15]. In contrast, rather mild treatment, i.e., being treated in flowing H_2 at 250°C for 2 h, is sufficient for the activation of $Ni_{85}P_{15}$ UAAP [7]. It seems reasonable to argue that more severe treatment might induce restructuring of

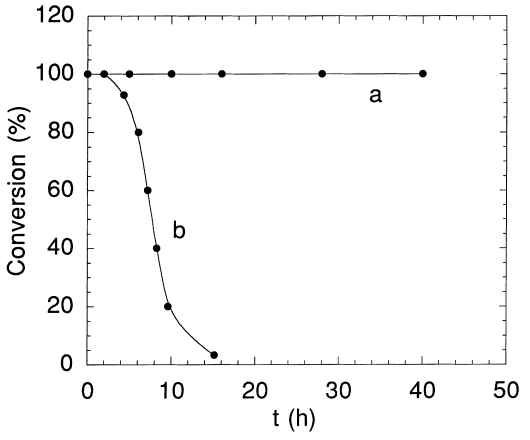

Fig. 6. Conversions of the hydrogenation of styrene versus time. Reaction temperature and liquid space velocity were (a) $Ni_{85}P_{15}$ UAAP, 433 K and 40 h^{-1}; (b) $Ni_{87}P_{13}$ ribbon, 553 K and 6 h^{-1}, respectively (from [7]).

the amorphous ribbon. In fact, it has been reported that the $Ni_{87}P_{13}$ ribbon sample was partially crystallized only after 10 h on stream [55]. Obviously, the relatively higher surface area and simple pretreatment conditions as well as the greater flexibility in controlling the composition of the amorphous alloys are the main advantages of the UAAP produced by chemical reduction over the corresponding ribbons prepared by quenching method. To further improve the stability and increase the surface area of the amorphous alloys, supported NiP and CoP amorphous alloy samples prepared by reduction methods have been developed by Deng et al. Their silica supported NiP sample has shown good stability and activity in the hydrogenation of styrene as compared with the amorphous ribbon sample or supported nickel catalyst. It has been suggested that if the preparation could be scaled-up, the supported amorphous catalysts might become a new class of industrial catalyst [19].

To investigate the influence of the surface aggregation state on catalytic properties, comparative studies have been done on the surface and catalytic properties of samples including a $Ni_{67}B_{33}$ UAAP catalyst (a-NiB), and its derivatives, i.e., partially crystallized (p-NiB) and crystalline (c-NiB) catalysts. The results are shown in Table 5 [56].

As can be seen from Table 5, the BET surface area follows the order of a-NiB>p-NiB>c-NiB, indicating that the thermal treatments result in both the sintering and the crystallization of the UAAP. Apparently, the differences in the conversion of ethylene and the hydrogen uptake of the three samples cannot be directly related to the growth of the particles, and interestingly, the turnover frequencies of them, i.e., the activities per surface Ni atom, are almost the same. The results are consistent with the conclusions derived by XPS, which reveal that the binding energies of the elementary nickel, boron atoms alloying with nickel (Bn) and boron oxide species (Bo) in the three samples remain almost unchanged. Furthermore, as can be seen in Table 5, the increase of the surface concentration of nickel species in p-NiB is accompanied by the decrease of the boron oxide species Bo. The results suggest that some of the surface nickel atoms originally covered by Bo species might be exposed by the heat treatment that caused the aggregation of the Bo species. It can be concluded that the different heat treatments (p-NiB at 573 K, and c-NiB at 773 K, respectively) not only result in the partial or total crystallization of the amorphous alloys but also induce the redistribution of the components. Thus, in comparison with a-NiB sample, the increase in the hydrogen uptake and the ethylene conversion of p-NiB can

Table 5
The influence of the surface aggregation state of $Ni_{67}B_{33}$ catalysts on their ethylene hydrogenation properties [56][a]

Catalyst	Surface area (m^2/g)	Conversion (%)	H_2 uptake (mol/g)	Relative TOF	Surface concentration[b]		
					Ni	Bn	Bo
a-NiB	19	50	23	1.00	63	8	29
p-NiB	15	88	41	0.99	74	9	17
c-NiB	8	24	11	1.00	67	16	17

[a]The ethylene hydrogenation reaction was carried out at 423 K, 0.1 MPa with a H_2 to ethylene ratio of 1.0 and at a weight hour space velocity=2400 h^{-1}.
[b]Surface concentration estimated by XPS.

be understood, even though its specific surface area is diminished due to sintering. Finally, the decrease of the surface concentration of Ni atoms and the increase of Bn in the c-NiB sample might correlate with the migration of Bn from bulk to surface during the heat treatment at a higher temperature (773 K) and the complete crystallization of the amorphous alloy. The existence of boron in the bulk phase of UAAP has been reported in [28]. In short, the active sites for the hydrogenation of ethylene in the amorphous and crystallized NiB particles are similar in nature but differ in number.

To explore the promoter effect of B and P in UAAP, comparative studies on NiP and NiB catalysts prepared by chemical reduction have been carried out recently by Deng et al. [57]. Listed in Table 6 are their results on the hydrogenation of 1,3-cyclopentadiene to cyclopentene catalyzed by the $Ni_{72}B_{28}$ and $Ni_{87}P_{13}$ catalysts. The reaction rate on $Ni_{72}B_{28}$ is an order of magnitude higher than that on $Ni_{87}P_{13}$. However, similar differences are found in the surface area and the number of nickel atoms on the surface of the two catalysts. Consequently, the turnover frequencies for hydrogen on them are in the same order of magnitude. The authors concluded that the differences in the hydrogenation rate of 1,3-cyclopentadiene to cyclopentene are mostly due to the differences in the number rather than the nature of the active sites on the surface of the NiB and NiP UAAP. Thus, the different electronic effects induced by B and P atoms [39] should not be the main reason for the different rates of the reaction. A comparative study on the catalytic properties of $Ni_{68}B_{32}$, $Ni_{83}P_{17}$ UAAP and pure nickel for the hydrogenation of ethylene has been conducted. Data on the apparent activation energy and the pre-exponential factor derived from Arrhenius equation based on reaction rates measured at different temperatures are shown in Table 2. The activation energies and the pre-exponential factors are in orders of NiP<NiB<Ni and NiP$\ll$NiB<Ni, respectively.

It is known that the activation energy and the pre-exponential factor of the reaction provide insights into the nature and the number of the active sites, respectively. The low A_s values for NiB and especially for NiP indicate that the number of active sites on NiB and especially on NiP are rather low, which should correlate to the low concentration of surface metal atoms, due to, as discussed in the above section, the existence of the oxides or the enrichment of the metalloid elements on the surface. It is noteworthy that B and P atoms have shown similar effects in lowering the activation energy, and this indicates that the electric charge transfer between them and the metal ions, if there is any, should go in the same direction.

It appears that the surface state of the NiP or NiB catalysts is critical in their application. How to avoid the surface of the catalyst being covered by inert species rather than the metal atoms should be seriously considered, even at the expense of losing the completely amorphous state of these kinds of catalysts. In addition, it appears that B and P have shown noticeable effects in decreasing the activation energy to different extents, and the potential application of either individual or the combination of them in improving the activity of catalysts in various hydrogenation reactions might be expected.

The fact that amorphous catalysts have superior selectivities or higher activities than the conventional crystalline catalyst has been reviewed elsewhere [2]. Listed in Table 7 are results of the hydrogenation of CO catalyzed by the NiB, NiP, NiPB and FeB UAAP

Table 6
Catalytic properties of UAAP of NiB and NiP[a] [57]

Catalyst	Surface area of Ni (m^2/g)[b]	Surface Ni atoms/g cat	Reaction rate (mol H_2/(g cat s))	TOF (s^{-1})
$Ni_{72}B_{28}$	29.7	4.57×10^{20}	4.68×10^{-4}	0.617
$Ni_{87}P_{13}$	2.78	4.28×10^{19}	6.43×10^{-5}	0.906

[a]The catalytic reaction was the hydrogenation of 1,3-cyclopentadiene (1.35×10^{-3} mol dm^{-3}) to cyclopentene at 25°C in 99% ethanol. The initial hydrogen pressure was 1.0 MPa that dropped linearly with time in the range 1.0–0.4 MPa. The reaction rates listed in the table were calculated from the reaction time when the pressure decreased from 0.8 to 0.6 MPa.
[b]Surface area of nickel measured by hydrogen adsorption.

Table 7
Conversion and the distribution of products by the hydrogenation of CO at 573 K, 0.1 MPa, with $H_2/CO=2$ and F/W=5400 ml/h

Catalyst	CO conversion (wt%)	C_1	C_2–C_4	C_2–C_3 olefin
$Ni_{67}B_{33}$	50.0	31.5	68.5	
$Ni_{73}P_{11}B_{16}$	19.8	19.3	80.7	
$Ni_{83}P_{17}$	12.4	11.0	89.0	
$Ni_{67}B_{33}$[a]	96.6	100		
$Fe_{80}B_{20}$	10.0	71.0		29.0
$Fe_{68}B_{32}$	3.0	31.0		69.0
$Fe_{60}B_{40}$	3.0	26.0		74.0
$Fe_{81}B_{13.5}Si_{3.5}C_2$[b]	0.1	56.0		44.0

[a]Completely crystallized sample.
[b]Amorphous ribbon sample.

catalysts. These catalysts are not only more active than the ribbon samples but also very selective as compared with conventional catalysts. The selectivity of C_2–C_4 hydrocarbons can reach as high as 89% for the $Ni_{83}P_{17}$ catalyst, while comparatively the $Ni_{66}B_{33}$ has a higher conversion but lower selectivity, and furthermore produces only methane after it has been completely crystallized. Interestingly, under the same reaction conditions, the main products shift to C_2–C_3 olefins when FeB UAAP are used to replace NiB as catalysts, and the selectivity of the FeB catalyst increases with the increase of its boron content and reaches 74% for the $Fe_{60}B_{40}$ catalyst. In contrast to the conventional crystalline catalyst, the hydrocarbons produced on the above catalysts are apparently higher than the value expected by the Schulz–Flory distribution law (C_2–C_5 components <55%) [55].

Based on the understanding of the catalytic properties of the binary UAAP systems, and by taking the advantage of chemical reduction method, which gives an adjustable product composition, some ternary UAAP catalysts with better catalytic properties have been explored with promising success. The $Ni_{73}P_{11}B_{16}$ UAAP listed in Table 7 is an example in this respect. Indeed, as a hybrid of the NiB and NiP samples, the NiPB have shown rather good selectivity and high conversion concurrently. Moreover, it has been reported that NiP UAAP have a higher thermal stability than that of NiB [57], and interestingly the thermal stability of NiPB UAAP is higher than both NiB and NiP, i.e., $Ni_{73}P_{11}B_{16}$> $Ni_{90}P_{10}$>$Ni_{67}B_{33}$ [58]. Ternary UAAP, which consists of one metalloid element and two metals, have also shown promising properties. For example, it is known that $Ni_{32.5}Co_{31.7}B_{35.8}$ UAAP have a much higher activity than Raney nickel in the hydrogenation of benzene with cyclohexane as the only product [28]; and by adding a small amount of W into NiP UAAP, the catalytic properties of the $Ni_{86.9}W_{0.14}P_{13}$ catalyst are dramatically different from those of $Ni_{86}P_{14}$ UAAP in the hydrogenation of cyclopentadiene and cyclopentene [29].

As described above, the unusual properties of the UAAP and the possibilities of adjusting their composition and structure through chemical preparation have shown exciting prospects for the future application of these kinds of new materials in catalysis. The application of UAAP as catalysts in reactions carried out in liquid phase under moderate temperature seems promising, e.g., the hydrogenation reactions in producing some fine chemicals. By proper selection of the constituents and the preparation conditions, the possibilities in tailoring the properties of catalysts to meet the need of various reactants are open. Despite the progress in the preparation, characterization and application of UAAP, the present situation in this area is, to our understanding, more a practical experience than theoretical understanding, and more a speculation, even a conflicting explanation, than a scientific prediction. The mechanistic study and search of new approaches to the chemical preparation of UAAP, the characterization of the UAAP under in situ reaction conditions to get a deeper insight on the basic rules in designing the surface of catalysts, the exploration of UAAP with unique catalytic properties in comparison with the conventional catalysts, and similar investigations on the ultrafine amorphous oxide catalysts are challenging tasks, which require further cooperation between chemists, physicists, and engineers to bring this interdisciplinary field to the forefront of science and technology [3].

Acknowledgements

This paper is finalized in the summer of 1997 during the author's visit to UW-Madison on his sabbatical leave. Special thanks to Professor J.A. Dumesic for his

helpful discussions on subjects of our common interest and his hospitality making the visit fruitful. We also thank Professor J. Deng of Fudan University for providing the reprints of his papers and his helpful discussions. The author is grateful to his coworkers in the Chemistry Department of NJU: Professors J. Shen, Y. Fan, Z. Hu and Q. Yan for their contributions to the studies reviewed in this paper and their help in the preparation of this manuscript.

References

[1] W.L. Johnson, Progr. Mater. Sci. 30 (1986) 81.
[2] A. Molnar, G.V. Smith, M. Bartók, Adv. Catal. 36 (1989) 329.
[3] G.C. Hadjipanayis, R.W. Siegel (Eds.), Nanophase Materials, Synthesis–Properties–Applications, NATO ASI Series, Kluwer Academic Publishers, Dordrecht, 1996.
[4] D.L. Bourell (Ed.), Synthesis and Processing of Nanocrystalline Powder, The Minerals, Metal, Materials Society, 1994.
[5] A. Inoue, J. Saida, T. Masumoto, Metal. Trans. 19A (1988) 2315.
[6] S. Linderoth, S. Mørup, J. Appl. Phys. 69(8) (1991) 5256.
[7] J. Shen, Z. Li, Q. Zhang, Y. Chen, Q. Bao, Z. Li, in: L. Guczi, F. Solymosi, P. Tetenyi (Eds.), New Frontiers in Catalysis, Akademiai1 Kiado, Budapest, 1993, p. 2193.
[8] J. Ding, W.F. Miao, T. Tsuzuki, P.G. McCormick, R. Street, in: D.L. Bourell (Ed.), Synthesis and Processing of Nanocrystalline Powder, The Minerals, Metal, Materials Society, 1994, p. 69.
[9] H. Schlesinger, H.C. Brown, A.E. Finholt, J.R. Gilbreath, H.R. Hoekstra, H.R. Hyde, J. Am. Chem. Soc. 75 (1953) 215.
[10] J. van Wonterghem, S. Mørup, C.J.W. Koch, S.W. Charles, S. Wells, Nature 322 (1986) 622.
[11] J. Saida, A. Inoue, T. Masumoto, Metall. Trans. A 22A (1991) 2125.
[12] J.Y. Shen, Z.Y. Li, Q.J. Yan, Y. Chen, J. Phys. Chem. 97 (1993) 8564.
[13] S. Linderoth, S. Mørup, J. Appl. Phys. 67 (1990) 4472.
[14] A. Yokoyama, H. Komiyama, H. Inoue, T. Masumoto, H.M. Kimura, J. Catal. 68 (1981) 355.
[15] J. Deng, X. Zhang, Appl. Catal. 37 (1988) 339.
[16] Z. Hu, J.Y. Shen, Y. Chen, M. Lu, Y.F. Hsia, J. Non-crystalline Solids 159 (1993) 88.
[17] Z. Hu, J. Shen, Y. Fan, Y. Hsia, Y. Chen, J. Mater. Sci. Lett. 12 (1993) 1020.
[18] J. Shen, Q. Zhang, Z. Li, Y. Chen, J. Mater. Sci. Lett. 15 (1996) 715.
[19] J. Deng, X. Zhang, Solid State Ionics 32 33 (1989) 1006.
[20] J.Y. Shen, Z. Hu, Y.F. Hsia, Y. Chen, J. Phys. 4 (1992) 6381.
[21] Z. Hu, Y. Chen, Y.F. Hsia, Nucl. Instrum. Meth. Phys. Res. B 76 (1993) 121.
[22] Z. Hu, Y. Fan, Y. Wu, Q. Yan, Y. Chen, J. Magn. Magn. Mater. 104–144 (1995) 413.
[23] J. Shen, Z. Hu, Q. Zhang, L. Zhang, Y. Chen, J. Appl. Phys. 71 (1992) 5217.
[24] J.-G. Zhang, J. Mater. Eng. Perform. 4 (1995) 453.
[25] S. Mørup, S.A. Sethi, S. Linderoth, C. Bender Koch, M.D. Bentzon, J. Mater. Sci. 27 (1992) 3010.
[26] T. Uehori, A. Hosaka, Y. Tokuoka, T. Izumi, Y. Imaoka, IEEE Trans. Mag. MAG-14(1978) 852.
[27] I. Dragieva, G. Gavrilov, D. Buchkov, M. Slavcheva, J. Less-Common Metals 67 (1979) 375.
[28] H. Wang, Z. Yu, H. Chen, J. Yang, J. Deng, Appl. Catal. A 129 (1995) L143.
[29] J.F. Deng, H.Y. Chen, J. Mater. Sci. Lett. 12 (1993) 1508.
[30] K.J. Klabunde, J.V. Stark, O. Koper, C. Mohs, A. Khaleel, G. Glavee, D. Zhang, C.M. Sorenson, G.C. Hadjipanayis, in: G.C. Hadjipanayis, R.W. Siegel (Eds.), Nanophase Materials, Synthesis–Properties–Applications, NATO ASI Series, Kluwer Academic Publishers, Dordrecht, 1996, p. 1.
[31] A. Levy, J.B. Brown, C.J. Lyons, Ind. Eng. Chem. 52 (1960) 211.
[32] R.N. Duncan, T.L. Arney, Plating Surf. Finish. 71 (1984) 49.
[33] J. Shen, Z. Li, Q. Wang, Y. Chen, J. Mater. Sci. 32 (1997) 749.
[34] Z. Hu, Y. Fan, F. Chen, Y. Chen, J. Chem. Soc., Chem. Commun. (1995) 247.
[35] G.L. Rochfort, R.D. Rieke, Inorg. Chem. 25 (1986) 348.
[36] Z. Hu, Y. Han, Y. Fan, Y. Chen, Chinese Patent 96117127.8.
[37] Z. Hu, J. Shen, Y. Chen, Y. Hsia, H. Zhai, J. Magn. Magn. Mater. 104–107 (1992) 583.
[38] C.R. Shipley Jr., Plating Surf. Finish. 71 (1984) 92.
[39] Y. Okamoto, Y. Nitta, T. Imanaka, S. Teranishi, J. Chem. Soc., Faraday Trans. I 75 (1979) 2027.
[40] S. Sada, Kogyo Kagaku Zasshi 71 (1968) 957.
[41] J. Shen, Z. Hu, L. Zhang, Z. Li, Y. Chen, Appl. Phys. Lett. 59 (1991) 3545.
[42] Z. Hu, Y. Hsia, J. Zheng, J. Shen, Q. Yan, L. Dai, J. Appl. Phys. 70(1) (1991) 436.
[43] Y. Fan, Z. Hu, Z. Xu, Y. Chen, Chem. J. Chin. Univ. 15 (1993) 117.
[44] Y.C. Guo, Z.C. Wang, Non-crystalline Physics, Science Press, Beijing, 1984.
[45] R.C. O'Handley, R. Hasegawa, R. Ray, C.P. Chou, Appl. Phys. Lett. 29 (1976) 330.
[46] H. Yamashita, M. Yoshikawa, T. Funabiki, S. Yoshida, J. Chem. Soc., Faraday Trans. I 81 (1985) 2485.
[47] H. Yamashita, M. Yoshikawa, T. Funabiki, S. Yoshida, J. Chem. Soc., Faraday Trans. I 82 (1986) 1771.
[48] T. Imanaka, J. Tamakai, S. Teranish, Chem. Lett. (1984) 449.
[49] T. Imanaka, J. Tamakai, S. Teranish, Nippon Kagaku Kaishi (1985) 1064.
[50] T. Imanaka, J. Tamakai, Chem. Lett. (1986) 679.
[51] W.S. Xia, Y. Fan, Y.S. Jiang, Y. Chen, Appl. Surf. Sci. 103 (1996) 1.
[52] J. Shen, B.E. Spiewak, J.A. Dumesic, Langmuir 13 (1997) 2735.

[53] S. Yoshita, H. Yamashita, T. Funabiki, T. Yonezawa, J. Chem. Soc., Faraday Trans. I 80 (1984) 1435.
[54] W.S. Xia, Z. Hu, Y.S. Jiang, Y. Chen, J. Mol. Struct. 366 (1996) 259.
[55] B. Zhong, E. Min, S. Dong, J. Deng, Acta Chim. Sinica 47 (1989) 1052.
[56] Y. Fan, Z. Hu, J. Shen, Q. Yan, Y. Chen, J. Mater. Sci. Lett. 12 (1993) 596.
[57] J. Deng, J. Yang, S. Sheng, H. Chen, G. Xiong, J. Catal. 150 (1994) 434.
[58] Y. Fan, Z. Hu, Z. Xu, Y. Chen, Chem. J. Chin. Univ. 15 (1994) 117.